Mahbub, Md. Selim; Kamleh, Waseem Rolf; Leinweber, Derek Bruce; Moran, Peter John; Williams, Anthony Gordon

Low-lying odd-parity states of the nucleon in lattice QCD

Physical Review. D. Particles, Fields, Gravitation and Cosmology, 2013; 87(1):011501

http://prd.aps.org/abstract/PRD/v87/i1/e011501

PHYSICAL REVIEW D **87,** 011501(R) (2013)

Low-lying odd-parity states of the nucleon in lattice QCD

M. Selim Mahbub, Waseem Kamleh, Derek B. Leinweber, Peter J. Moran, and Anthony G. Williams

Special Research Centre for the Subatomic Structure of Matter, School of Chemistry and Physics, University of Adelaide, Adelaide, South Australia 5005, Australia

(Received 3 September 2012; published 28 January 2013)

The odd-parity nucleon spectrum is examined in the light quark-mass regime in $2+1$ flavor lattice QCD. Configurations generated by the PACS-CS Collaboration and made available through the International Lattice Data Grid are used, with the lightest pion mass at 156 MeV. A novel method for tracking the individual energy eigenstates as the quark mass changes is introduced. The success of this approach reveals the flow of the states towards the physical masses. Using the correlation-matrix method, the two lowest-energy states revealed are found to be in accord with the physical spectrum of nature.

DOI: 10.1103/PhysRevD.87.011501 PACS numbers: 11.15.Ha, 12.38.Gc

Lattice QCD is the only currently known *ab initio* or first-principles approach to the fundamental quantum field theory governing the properties of hadrons, quantum chromodynamics (QCD). While the ground-state hadron spectrum of QCD is well understood, a determination of the excited state energy spectrum is in the process of being revealed.

Hadron spectroscopy is dependent on the rich dynamics of the strong interaction. For example, the experimentally observed mass of the first positive-parity excitation of the nucleon, known as the Roper resonance, $N\frac{1}{2}^+$ (1440) P_{11}, is surprisingly low compared to the lowest-lying negative-parity partner $N\frac{1}{2}^-$ (1535) S_{11}. This phenomenon is not observed in constituent or valence quark models where the lowest-lying odd-parity state occurs naturally *below* the first $J^P = \frac{1}{2}^+$ excitation.

Drawing on experimental results, we note that the Breit-Wigner width of the $N^-(1535)$ state is ≈ 150 MeV, approximately half the width of the Roper $N^+(1440)$ [1]. Furthermore, the branching fraction $\Gamma(\pi N)/\Gamma$ for $N^-(1535)$ is $2/3$ of the Roper. Together, these factors indicate a suppression of $1/3$ in the coupling of πN to the $N^-(1535)$ state relative to the Roper. Noting that the light πN dressing makes the most important self-energy contribution, it is anticipated that the self-energy dressings of πN for the $N^-(1535)$ will be reduced to approximately 10% of that for the Roper. A consequence of this is to suppress the finite-volume effects of the lattice QCD simulation which can otherwise lead to large energy shifts associated with the avoidance of energy-level crossings of the single and multiparticle scattering states. Similar arguments for the $N^-(1650)$ suggest πN self-energy contributions are suppressed to the 25% level. Thus, it is interesting to directly compare the results of our lattice QCD simulations with experiment and gain insight on the quark-mass dependence of these states.

The experimentally observed nearly degenerate S_{11} (1535) and (1650) states are in agreement with the simple quark-model predictions based on SU(6) symmetry. Therefore, looking at the low-lying $N\frac{1}{2}^-$ energy states and their structure from the first-principles approach is potentially very revealing. Some recent full QCD results can be seen in Refs. [2–7]. Herein, it will be interesting to explore the physics associated with the dynamical fermion loops of full QCD, this time at very light quark masses.

The spectrum of the $N\frac{1}{2}^-$ states is dense. Thus it is important to adopt a method that can isolate the individual states that are otherwise close in energy. The variational method [8,9] is the state-of-the-art approach for achieving this in lattice hadron-spectroscopy calculations. Through a generalized eigenvalue analysis of a matrix of correlation functions, the process enables one to create highly optimized interpolating fields designed to excite a single energy eigenstate of the QCD Hamiltonian. The masses of the energy states are then obtained through a standard effective-mass analysis [10] providing a robust approach for extracting the energy states at early Euclidean times.

In this paper, we utilize the established approach of Refs. [6,7] to explore the low-lying $N\frac{1}{2}^-$ energy states in full QCD. In doing so, a novel method has been developed to track the energy eigenstates from heavy to light quark masses. The method is particularly useful when the energy states are nearly degenerate.

The two-point correlation-function matrix for $\vec{p} = 0$ can be written as

$$G_{ij}^{\pm}(t) = \sum_{\vec{x}} \mathrm{Tr}_{\mathrm{sp}}\{\Gamma_{\pm}\langle\Omega|\chi_i(x)\bar{\chi}_j(0)|\Omega\rangle\} = \sum_{\alpha} \lambda_i^{\alpha}\bar{\lambda}_j^{\alpha} e^{-m_\alpha t}, \quad (1)$$

where Dirac indices are implicit, λ_i^{α} and $\bar{\lambda}_j^{\alpha}$ are the couplings of interpolators χ_i and $\bar{\chi}_j$ at the sink and source, respectively, α enumerates the energy eigenstates with mass m_α, and $\Gamma_{\pm} = (\gamma_0 \pm 1)/2$ projects the parity of the eigenstates. A linear superposition of interpolators $\bar{\phi}^{\alpha} = \sum_j \bar{\chi}_j u_j^{\alpha}$ creating state α provides the relationship

$$G_{ij}(t_0 + \triangle t)u_j^{\alpha} = e^{-m_\alpha \triangle t} G_{ij}(t_0)u_j^{\alpha}, \quad (2)$$

from which right and left eigenvalue equations are obtained:

$$[(G(t_0))^{-1}G(t_0+\triangle t)]_{ij}u_j^\alpha = c^\alpha u_i^\alpha, \quad (3)$$

$$v_i^\alpha[G(t_0+\triangle t)(G(t_0))^{-1}]_{ij} = c^\alpha v_j^\alpha, \quad (4)$$

with $c^\alpha = e^{-m_\alpha \triangle t}$. The vectors u_j^α and v_i^α diagonalize the correlation matrix at time t_0 and $t_0+\triangle t$ making the projected correlation matrix $v_i^\alpha G_{ij}^{\pm}(t)u_j^\beta \propto \delta^{\alpha\beta}$. The parity and eigenstate projected correlator

$$G_\pm^\alpha \equiv v_i^\alpha G_{ij}^{\pm}(t)u_j^\alpha \quad (5)$$

is then analyzed to obtain masses of energy states. We note that the large Euclidean time behavior of the projected correlation functions and associated effective-mass plateaus demonstrate the presence of a single state.

An eigenvector analysis of a symmetric matrix having orthogonal eigenvectors can be constructed by inserting $G(t_0)^{-\frac{1}{2}}G(t_0)^{\frac{1}{2}} = I$ in Eq. (3) and multiplying by $G(t_0)^{\frac{1}{2}}$ from the left:

$$G(t_0)^{-\frac{1}{2}}G(t_0+\triangle t)G(t_0)^{-\frac{1}{2}}G(t_0)^{\frac{1}{2}}u^\alpha = c^\alpha G(t_0)^{\frac{1}{2}}u^\alpha, \quad (6)$$

$$G(t_0)^{-\frac{1}{2}}G(t_0+\triangle t)G(t_0)^{-\frac{1}{2}}w^\alpha = c^\alpha w^\alpha, \quad (7)$$

where $w^\alpha = G(t_0)^{\frac{1}{2}}u^\alpha$ and $[G(t_0)^{-\frac{1}{2}}G(t_0+\triangle t)G(t_0)^{-\frac{1}{2}}]$ is a real symmetric matrix, with orthogonal eigenvectors w^α. The vector u^α may be recovered from the w^α via $u^\alpha = G(t_0)^{-\frac{1}{2}}w^\alpha$.

The PACS-CS 2 + 1 flavor dynamical-fermion configurations [11] made available through the International Lattice Data Grid [12] are used herein. These configurations use the nonperturbatively $\mathcal{O}(a)$-improved Wilson fermion action and the Iwasaki-gauge action [13]. The lattice volume is $32^3 \times 64$, with $\beta = 1.90$ providing a lattice spacing of $a = 0.0907$ fm and a physical volume of $\approx (2.90\ \text{fm})^3$. Five values of the (degenerate) up and down quark masses are considered, with hopping parameter values of $\kappa_{ud} = 0.13700$, 0.13727, 0.13754, 0.13770 and 0.13781, corresponding to pion masses of $m_\pi = 0.702$, 0.572, 0.413, 0.293, 0.156 GeV [11]; for the strange quark $\kappa_s = 0.13640$. Gauge-invariant Gaussian smearing [14] is used at the fermion source and sink with a fixed smearing fraction and four different smearing levels including 16, 35, 100, and 200 sweeps [6,7].

We consider 350 configurations for the four heavier quarks and 198 configurations for the lightest quark. An ensemble of 750 samples for the lightest quark mass is created by using multiple fermion sources on each configuration, spaced to sample approximately independent regimes of each configuration. $\mathcal{O}(a^2)$ errors are expected to be small relative to the statistical errors [15,16].

The complete set of local interpolating fields with three different spin-flavor combinations for the spin-$\frac{1}{2}$ nucleon are considered herein:

$$\chi_1(x) = \epsilon^{abc}(u^{Ta}(x)C\gamma_5 d^b(x))u^c(x), \quad (8)$$

$$\chi_2(x) = \epsilon^{abc}(u^{Ta}(x)Cd^b(x))\gamma_5 u^c(x), \quad (9)$$

$$\chi_4(x) = \epsilon^{abc}(u^{Ta}(x)C\gamma_5\gamma_4 d^b(x))u^c(x). \quad (10)$$

Each interpolator has a unique Dirac structure giving rise to different spin-flavor combinations. Moreover, as each spinor has upper and lower components, with the lower components containing an implicit derivative, different combinations of zero-, one- and two-derivative interpolators are provided. The interpolator χ_4 is the time component of the local spin-$\frac{3}{2}$ isospin-$\frac{1}{2}$ interpolator which also couples to spin-$\frac{1}{2}$ states. It provides a different linear combination of zero- and two-derivative terms complementary to χ_1.

In Fig. 1, projected masses of the $N\frac{1}{2}^-$ states are presented from a 4×4 correlation matrix constructed from the interpolator χ_1 and four different smearing levels. The dependence of the results on the variational parameters t_0 and $\triangle t$ is illustrated. While the lowest energy state is almost independent of t_0 and $\triangle t$, the excited states show some dependence at smaller t_0 and $\triangle t$ values. As explained in Ref. [6], the energy states at $(t_0, \triangle t) = (18, 2)$ provide the best balance between the systematic and statistical uncertainties and these parameters are therefore selected for our numerical study.

In Fig. 2 we show results for the lowest energy state from dynamical and quenched [17] QCD simulations. As anticipated, the quenched and dynamical results are in agreement in the heavy quark-mass region. However, in the light quark-mass regime the results are significantly different as the effects of the light sea quarks become increasingly important. Only the dynamical results approach the physical value and this provides strong evidence for the nontrivial role of light sea-quark degrees of freedom to the structure of nature's hadron spectrum.

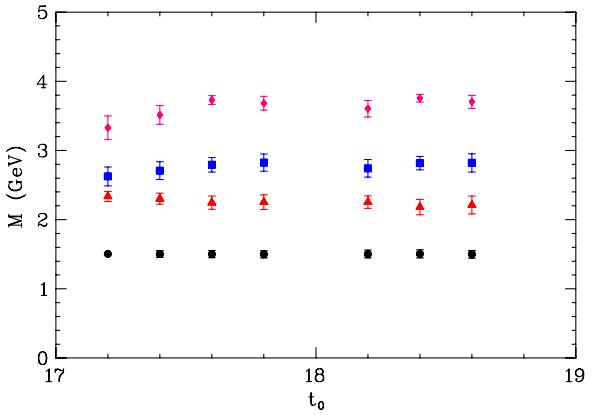

FIG. 1 (color online). $N\frac{1}{2}^-$ energy states from a 4×4 correlation-matrix analysis of the χ_1 interpolator at the lightest pion mass of $m_\pi = 156$ MeV. The variational parameters t_0 and $\triangle t$ are shown at the major and minor tick marks, respectively. For example, the leftmost points have $t_0 = 17$ and $\triangle t = 1$.

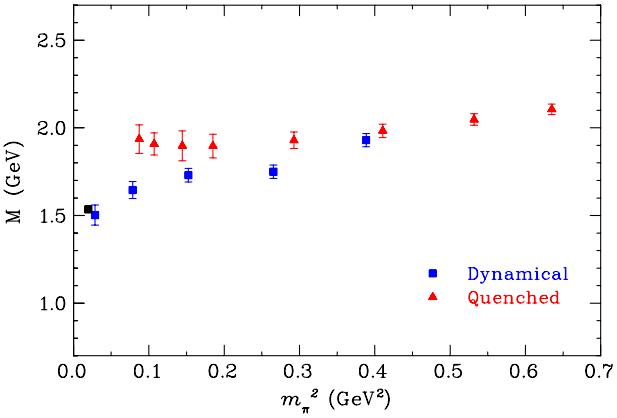

FIG. 2 (color online). Dynamical and quenched results for the lowest $N\frac{1}{2}^-$ energy state using the χ_1 interpolator.

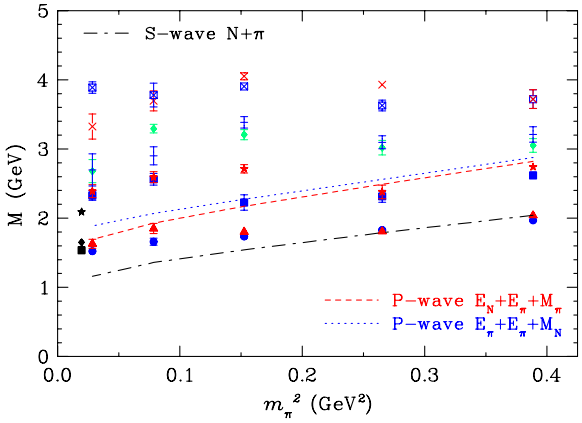

FIG. 3 (color online). $N\frac{1}{2}^-$ energy states from an 8×8 correlation matrix of χ_1 and χ_2 interpolators, for the pion mass range of 156–702 MeV. The physical $N\frac{1}{2}^-$ spectrum [1] is shown at the far left.

To explore the nearby second energy state $S_{11}(1650)$, we extend our analysis to include the interpolators χ_2 and χ_4 with a variety of smearing levels. The results of an 8×8 correlation-matrix analysis of χ_1 and χ_2 interpolators with four levels of smearing are presented in Fig. 3.

The trend of the lowest two energy states is in agreement with the physical values. The results at the two heaviest pion masses sit close to the scattering S-wave $N + \pi$ threshold; however, in the light quark-mass region these states move above the threshold. The consideration of five-quark interpolators is highly desirable for future investigations [18]. A similar situation prevails for the second pair of states in the spectrum, where the states sit close to the P-wave $E_N + E_\pi + M_\pi$ and $E_\pi + E_\pi + M_N$ threshold scattering states with back-to-back momenta of one lattice unit, $\vec{p} = (2\pi/L_x, 0, 0)$. The apparent flow of these states in the light-quark region toward the physical $S_{11}(2090)$ state is also interesting.

In presenting the results of Fig. 3 and assigning symbols to each of the energy levels observed at a particular quark mass, it is necessary to track the evolution of the states from one quark mass to the next. We have done this through a consideration of the evolution of the eigenvectors as the quark mass is changed.

Consider M interpolating fields making an $M \times M$ parity-projected correlation matrix $G(t)$ and its associated symmetric generalized eigenvalue equation of Eq. (7). Using the normalization $\sum_i^M |w_i^\alpha|^2 = 1$, the quantity $\vec{w}^\alpha(m_q) \cdot \vec{w}^\beta(m_q) = \delta_{\alpha\beta}$. This feature enables the use of the generalized measure

$$\mathcal{W}^{\alpha\beta}(m_q, m_{q'}) = \vec{w}^\alpha(m_q) \cdot \vec{w}^\beta(m_{q'}) \tag{11}$$

to identify the states most closely related as we move from quark mass m_q to an adjacent quark mass $m_{q'}$. The state numbers α and β are assigned in order of increasing projected eigenstate energy at the quark masses m_q and $m_{q'}$, respectively. Typical results for this generalized measure of eigenvector overlap are presented in Table I.

For each value of state index α there is only one value of β where the magnitude of the entry is significantly larger than all others and approaching unity. The most relevant entries for consideration are the immediate neighbors of α where a crossing of the eigenvectors moves the largest entry off the diagonal.

This measure provides a clear identification of how states in the spectrum at quark mass m_q are associated

TABLE I. The scalar product $\vec{w}^\alpha(m_q) \cdot \vec{w}^\beta(m_{q'})$ for $\kappa = 0.13754$ ($m_\pi = 413$ MeV) and $\kappa' = 0.13770$ ($m_\pi = 293$ MeV) for an 8×8 correlation matrix of χ_1 and χ_2 with four different levels of smearing. State numbers α and β correspond to row and column number, respectively.

0.91	0.40	0.02	0.02	0.01	−0.05	0.00	0.00
0.40	**−0.91**	0.00	0.01	−0.02	0.01	−0.01	0.00
−0.01	−0.01	**0.96**	−0.27	0.01	−0.01	0.00	0.02
−0.03	0.00	0.27	**0.96**	0.01	0.01	0.02	0.00
0.04	0.03	0.01	−0.01	−0.22	**0.97**	0.02	0.01
0.01	−0.01	−0.01	−0.01	**0.98**	0.22	0.04	0.00
0.00	0.00	−0.02	0.01	0.01	−0.01	−0.12	**0.99**
0.01	−0.01	0.00	−0.02	−0.04	−0.03	**0.99**	0.12

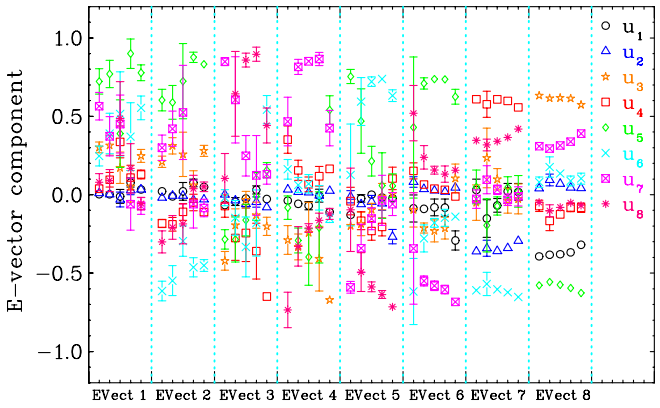

FIG. 4 (color online). The components of the eigenvector u^α providing the amplitude for each interpolating field at the source for creating the state α. The states are labeled by the eigenvector (EVect) number with the ordering as provided in Fig. 3 at the heaviest quark mass. For each EVect, the eigenvector components are plotted from left to right in order of increasing quark mass. In the legend, (u_1, u_2), (u_3, u_4), (u_5, u_6) and (u_7, u_8) correspond to the smearing-sweep levels of 16, 35, 100 and 200, respectively. Odd numbers in the subscripts correspond to the contribution from the χ_1 interpolator, whereas even numbers correspond to χ_2.

with states at the next value of quark mass, $m_{q'}$. For example, the results of Table I indicate the first four states at $m_{q'}$ appear with the same ordering in the spectrum as observed at m_q, the fifth state at $m_{q'}$ is associated with the sixth state at m_q and vice versa and similarly for the seventh and eighth states. We note that while the central values of the energies have changed order, the error bars are sufficiently large that one cannot conclude that an avoided energy level crossing has taken place in moving from quark mass m_q to $m_{q'}$.

The components of the eigenvector u^α, providing the amplitude for each interpolating field at the source for creating the state α, are provided in Fig. 4. A nontrivial contribution from both the χ_1 and χ_2 interpolators for the

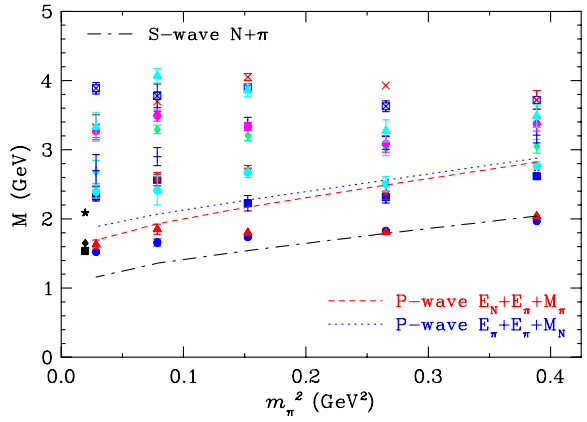

FIG. 5 (color online). Masses of 12 low-lying $N\frac{1}{2}^-$ energy states from two 8×8 correlation matrices of χ_1, χ_2 and χ_1, χ_4.

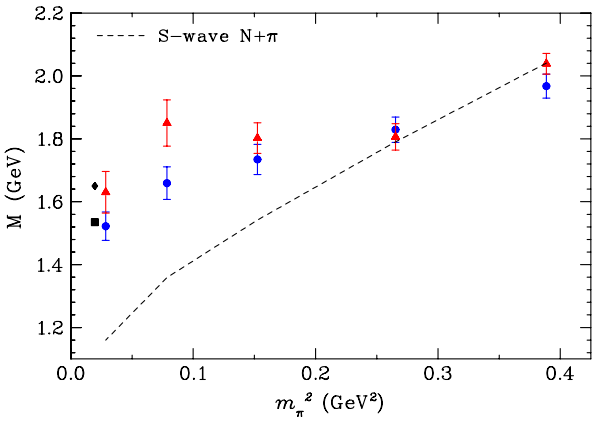

FIG. 6 (color online). The quark-mass dependence of the lowest two lowest-lying $N\frac{1}{2}^-$ states are compared with the S-wave scattering threshold.

lowest two energy states is evident. The scalar-diquark interpolator χ_1 dominates the lowest energy state. On the other hand, both χ_1 and χ_2 interpolators have large contributions to the second energy state where their strengths appear with opposite signs. The eigenvector components typically display a slow evolution as the quark mass is changed.

The energy states for our complete analysis are presented in Fig. 5. The results are drawn from two 8×8 correlation-matrix analyses for pairs of χ_1, χ_2 and χ_1, χ_4. The matrices are formed with each interpolator having four levels of smearing. Whereas the χ_1, χ_2 and χ_2, χ_4 analyses reveal a similar spectrum, four new states are revealed in the χ_1, χ_4 analysis providing the resolution of 12 low-lying states in our analysis.

In the SU(6) quark model, the odd-parity (1535) and (1650) states belong to the negative-parity, $L = 1$, 70-plet representation and have a small splitting associated with their different spin configurations [17]. The lowest two energy states revealed here are similarly close in mass, as illustrated in Fig. 5, in accord with the SU(6) quark model.

These two lowest-lying $N\frac{1}{2}^-$ states are presented in Fig. 6 in comparison with the S-wave scattering threshold. These lattice results, providing the first examination of the odd-parity nucleon spectrum at a pion mass as low as 156 MeV, display agreement with the physical values. Table II reports the eigenstate energies of the first six states.

TABLE II. Eigenstate energies (GeV) for the low-lying $N\frac{1}{2}^-$ states.

m_π^2	St.1	St.2	St.3	St.4	St.5	St.6
0.388	1.97(4)	2.04(3)	2.62(5)	2.74(5)	2.77(6)	3.05(10)
0.265	1.83(4)	1.81(4)	2.31(9)	2.38(10)	2.50(11)	3.02(10)
0.152	1.73(5)	1.80(5)	2.22(11)	2.71(6)	2.67(7)	3.21(7)
0.078	1.66(5)	1.85(7)	2.56(8)	2.59(8)	2.43(21)	3.29(6)
0.028	1.52(4)	1.63(6)	2.33(7)	2.39(9)	2.39(9)	2.68(17)

Although both these low-lying states are quite similar at the two heaviest quark masses, their approach to the physical values in the light quark-mass region are different. Significant chiral curvature is evident, in particular for the second state. It will be interesting to explore the mass dependence of these states using effective field theory techniques and to repeat these studies on matched lattices of different volume when they become available. Future studies will endeavor to observe the multiparticle scattering states and determine the resonance parameters of these states from the first principles of QCD.

This research was undertaken on the NCI National Facility in Canberra, Australia, which is supported by the Australian Commonwealth Government. We also acknowledge eResearch SA for generous grants of supercomputing time. This research is supported by the Australian Research Council.

[1] K. Nakamura *et al.* (Particle Data Group), J. Phys. G **37**, 075021 (2010).
[2] J. M. Bulava *et al.*, Phys. Rev. D **79**, 034505 (2009).
[3] J. Bulava, R. Edwards, E. Engelson, B. Joó, H.-W. Lin, C. Morningstar, D. Richards, and S. Wallace, Phys. Rev. D **82**, 014507 (2010).
[4] G. P. Engel, C. B. Lang, M. Limmer, D. Mohler, and A. Schafer (BGR [Bern-Graz-Regensburg] Collaboration), Phys. Rev. D **82**, 034505 (2010).
[5] R. G. Edwards, J. J. Dudek, D. G. Richards, and S. J. Wallace, Phys. Rev. D **84**, 074508 (2011).
[6] M. S. Mahbub, W. Kamleh, D. B. Leinweber, P. J. Moran, and A. G. Williams (CSSM Lattice Collaboration), Phys. Lett. B **707**, 389 (2012).
[7] B. J. Menadue, W. Kamleh, D. B. Leinweber, and M. S. Mahbub, Phys. Rev. Lett. **108**, 112001 (2012).
[8] C. Michael, Nucl. Phys. **B259**, 58 (1985).
[9] M. Luscher and U. Wolff, Nucl. Phys. **B339**, 222 (1990).
[10] M. S. Mahbub, A. Ó Cais, W. Kamleh, B. G. Lasscock, D. B. Leinweber, and A. G. Williams, Phys. Lett. B **679**, 418 (2009).
[11] S. Aoki *et al.* (PACS-CS Collaboration), Phys. Rev. D **79**, 034503 (2009).
[12] M. G. Beckett, P. Coddington, B. Joó, C. M. Maynard, D. Pleiter, O. Tatebe, and T. Yoshie, Comput. Phys. Commun. **182**, 1208 (2011).
[13] Y. Iwasaki, Report No. uTHEP-118, 1983.
[14] S. Gusken, Nucl. Phys. B, Proc. Suppl. **17**, 361 (1990).
[15] S. Dong, F. Lee, K. Liu, and J. Zhang, Phys. Rev. Lett. **85**, 5051 (2000).
[16] J. M. Zanotti, B. Lasscock, D. B. Leinweber, and A. G. Williams, Phys. Rev. D **71**, 034510 (2005).
[17] M. S. Mahbub, W. Kamleh, D. B. Leinweber, A. O. Cais, and A. G. Williams, Phys. Lett. B **693**, 351 (2010).
[18] C. Morningstar, J. Bulava, J. Foley, K. Juge, D. Lenkner, M. Peardon, and C. Wong, Phys. Rev. D **83**, 114505 (2011).